Reconfigurable nonreciprocal excitation of propagating exchange spin waves in perpendicularly magnetized yttrium iron garnet thin films

Hanchen Wang,[1,2,3,*] Jinlong Wang,[1,*] Shuyao Chen,[4,*] Peng Chen,[5,*] William Legrand,[3,*] Yu Zhang,[5] Lutong Sheng,[1] Rundong Yuan,[1] Jilei Chen,[2,6] Guoqiang Yu,[5] Caihua Wan,[5] Xiufeng Han,[5] Tao Liu,[4] Jean-Philippe Ansermet,[6,7,†] and Haiming Yu[1,2,‡]

[1]*Fert Beijing Institute, MIIT Key Laboratory of Spintronics, School of Integrated Circuit Science and Engineering, Beihang University, Beijing 100191, China*

[2]*International Quantum Academy, Shenzhen 518055, China*

[3]*Department of Materials, ETH Zurich, 8093 Zurich, Switzerland*

[4]*National Engineering Research Center of Electromagnetic Radiation Control Materials, University of Electronic Science and Technology of China, Chengdu 610054, China*

[5]*Beijing National Laboratory for Condensed Matter Physics, Institute of Physics, University of Chinese Academy of Sciences, Chinese Academy of Sciences, Beijing 100190, China*

[6]*Shenzhen Institute for Quantum Science and Engineering, Southern University of Science and Technology, Shenzhen 518055, China*

[7]*Institute of Physics, École Polytechnique Fédérale de Lausanne (EPFL), 1015 Lausanne, Switzerland*

(Received 24 April 2023; revised 24 July 2023; accepted 20 September 2023; published 3 October 2023)

We report the nonreciprocal excitation of propagating forward volume exchange spin waves in yttrium iron garnet (YIG) thin film with perpendicular anisotropy by bringing the in-plane magnetization of $Co_{20}Fe_{60}B_{20}$ (CoFeB) nanowires to resonance. All-electric spin-wave spectroscopy is used to measure propagating spin waves in YIG subjected to out-of-plane external magnetic fields. The nonreciprocity can be reconfigured by inverting the in-plane magnetization of the CoFeB nanowires. The exchange spin waves achieved in the experiments have wavelengths down to about 150 nm and fast group velocities of up to 1.6 km/s, which can be accounted for with the dipole-exchange spin-wave dispersion of the forward volume mode. Micromagnetic simulations reproduce these experimental features, verifying that the key physics behind this nonreciprocity is the intrinsically chiral dynamic stray fields generated by the resonating CoFeB magnetization. Our results provide key insights into advanced and high-frequency magnonic devices.

DOI: 10.1103/PhysRevB.108.134403

I. INTRODUCTION

Exchange spin waves are the excitations of magnetic moments mediated by Heisenberg exchange interaction in magnetic material systems [1–10]. Exchange interaction dominates over dipolar interactions in spin-wave dynamics when the wavelength is below several hundreds of nanometers [10–18]. In integrated magnonic devices which rely on wave-vector-dependent detection, the wavelength has to be short and the group velocity high [7,19–24]. Recently, many efficient ways to excite the exchange spin waves have been proposed and experimentally demonstrated, such as the nonlinear effect [14,25–28], spin textures [15,29,30], interlayer interactions [11,31–35], terahertz pulses [36], etc. [37,38]. In addition, exchange spin waves are an ideal platform to investigate nonreciprocal effects or couplings between quasiparticles because the precession becomes circular in the exchange regime, which leads either to strong coupling or to zero coupling to other harmonic precessions, such as coherent magnons, surface phonons, and polarized photons [39–49]. Previous experimental and theoretical studies revealed how the exchange spin waves in a thin film can unidirectionally couple to top or bottom surface modes depending on the propagating direction, owing to the topological properties of the dipolar interaction. Theoretical studies shed light on other nontrivial features, such as the magnon trap, magnon accumulation, the skin effect, etc. [11,24,49–58]. Most previous studies focused on in-plane magnetized systems, while the forward volume (FV) exchange spin waves of out-of-plane magnetized films have rarely been experimentally studied, even though they are particularly suitable for designing two-dimensional functional magnonic devices in which spin-wave propagation can occur equally in all in-plane directions [59–67]. It is worth highlighting that a highly nonreciprocal magnetostatic-surface-wave-like (MSSW-like) mode was experimentally achieved in Ta/Py bilayer systems using out-of-plane magnetic fields. The key mechanisms behind this achievement are the tilted out-of-plane anisotropy induced by the Ta underlayer and the spin pumping effect at the Ta/Py interface [68].

In this paper, we fabricated $Co_{20}Fe_{60}B_{20}$ (CoFeB) nanowires on top of 30-nm-thick yttrium iron garnet (YIG) thin film with perpendicular magnetic anisotropy (PMA) to

*These authors contributed equally to this work.
†jean-philippe.ansermet@epfl.ch
‡haiming.yu@buaa.edu.cn

excite propagating short-wavelength FV spin waves. By using all-electric spin-wave spectroscopy (AESWS), propagating spin waves in YIG are excited by microwave antennas covering the in-plane magnetized CoFeB nanowire and detected by antennas covering distant CoFeB nanowires positioned on either side of the emission antenna, thus allowing us to observe nonreciprocity within a single device. The nonreciprocity can be reconfigured by switching the in-plane magnetization direction of the CoFeB nanowires. We have observed group velocities of up to 1.6 km/s at spin-wave wavelengths as low as 150 nm. A series of devices with different antenna separation distances demonstrated the long-distance propagation of short-wavelength spin waves in PMA thin films.

II. SAMPLE AND EXPERIMENT

The YIG films with perpendicular magnetic anisotropy (PMA) were epitaxially grown on (111)-oriented single-crystal $Gd_{2.6}Ca_{0.4}Ga_{4.1}Mg_{0.25}Zr_{0.65}O_{12}$ [substituted gadolinium gallium garnet (sGGG)] substrates by radio-frequency (RF) sputtering at room temperature followed by a postannealing process. Prior to sputtering, the ultrahigh-vacuum custom-built sputtering chamber had a base pressure of 5.0×10^{-8} Torr. In the sputtering process, the YIG films were grown at an RF power of 90 W and an Ar pressure of 7×10^{-3} Torr. The film thickness was controlled by the deposition time with a precalibrated deposition rate of about 0.11 Å/s. Afterward, the deposited YIG film was annealed at 800 °C for 3 h with a pure oxygen pressure of 15 mTorr. To check the YIG crystal quality and verify the thickness, x-ray diffractometry (XRD) and x-ray reflectrometry (XRR) measurements were performed, and the results are presented in Appendix A. By fitting the oscillations in the XRR profile, we can estimate the thickness of the YIG thin film to be around 32 nm. The apparent Laue fringes in the XRD near the main peak from the sGGG substrate indicate the good crystal quality of the YIG thin film. In addition, magnetic hysteresis loops were measured both in plane (IP) and out of plane (OOP) using a superconducting quantum interference device (SQUID; see Appendix B), from which one can find that the film has strong PMA and can be saturated along the OOP direction with an external field strength smaller than 10 mT. Finally, to characterize its magnetic Gilbert damping, linewidths as a function of frequency were obtained from ferromagnetic resonance (FMR) measurements, the details of which can be found in Appendix B. The extracted damping is about 2.36×10^{-3}, and the inhomogeneous contribution to the linewidth is about 11 Oe.

Nanoscale spin-wave devices were fabricated using e-beam lithography (EBL) and lift-off processes. Nanowires were firstly structured in e-beam resist by EBL and then developed. Afterwards, the whole chip was transferred into the sputtering to deposit the 30-nm-thick CoFeB thin film at room temperature. After lift-off, two stripline (STL) antennas made of Ti (10 nm)/Au (100 nm) were patterned and deposited directly on top of two CoFeB nanowires using the EBL alignment, e-beam evaporation, and lift-off. The widths of the antennas extended slightly beyond the nanowire edges in order to ensure that they were fully covered and protected against oxidation. Several devices with propagation distances between 2 and 5 μm with a step of 1 μm were fabricated. The optical microscope and scanning electron microscope (SEM) images are shown in Appendix C to provide detailed device information.

To efficiently measure the propagating spin waves, we use all-electric spin-wave spectroscopy (AESWS) with its key component being a vector network analyzer (VNA) (Rohde and Schwarz ZVA 40) with a frequency range up to 40 GHz. The external magnetic fields are supplied by a U-shaped magnet underneath the sample with a maximum magnetic field of 200 mT. Coherent excitation and detection of spin waves are supported by two microwave ground-signal-ground (GSG) probes with individual microwave cables connecting to the two ports from the VNA, which can provide and receive the radio frequency (RF) current for and from the STL antennas on the chip. The injected RF current generates a dynamic electromagnetic field underneath the antenna to excite spin waves and detect them via the inverse physical process. The detection can happen at both the excitation part and the receiver antenna. If the detection antenna is the same as the excitation one, namely, STL1 (STL2), the detected spin-wave spectra corresponds to the S_{11} (S_{22}) parameters of the VNA. If the detection is done for another antenna, namely, STL2 (STL1), rather than the excitation one, namely, STL1 (STL2), the detected spectra are the S_{12} (S_{21}) parameters that characterize spin-wave propagation. The excitation power used for this work was fixed at 0 dBm to obtain the best signal. Before all experiments, a large in-plane external magnetic field was applied to the whole system to align the magnetization of the CoFeB wire along its easy axis (y direction). During the experiments, we applied an out-of-plane magnetic field to saturate the YIG films. However, due to the relatively low field strength compared with the CoFeB shape anisotropy field, the magnetization in the CoFeB nanowire was only slightly tilted towards the out-of-plane direction. Consequently, the magnetization in the nanowires predominantly remained in plane throughout the measurements.

Before presenting the experimental results, we first introduce the key physical parameters of our experiments. Excitation in the CoFeB nanowires is done with STL antennas, and resonances are Kittel mode resonances with elliptical precession. The ellipticity $\mathcal{D}$ of the nanowire precession can be theoretically described as [49–51]

$$\mathcal{D} = \sqrt{\frac{H_{\text{ext}} + N_{xx}M_s}{H_{\text{ext}} + N_{yy}M_s}}, \tag{1}$$

where H_{ext} is the external magnetic field and the demagnetization factors are $N_{xx} \simeq w/(d+w)$ and $N_{yy} \simeq d/(d+w)$, where d is the thickness of nanowires and w is their width. If the width and thickness were equal, the precession would be circular. In our case, d is 30 nm and w is about 680 nm.

Once the CoFeB nanowire is excited, it generates dynamic stray fields, which in turn excite spin waves in the adjacent PMA YIG film at the same frequency. It is worth noting that the excited spin waves in YIG are short-wavelength ones because higher wave vector values in YIG are needed to keep the frequency the same in YIG and in CoFeB. Due to the spins in YIG pointing out of plane, only the x components of the dipolar fields generated by the CoFeB nanowire can

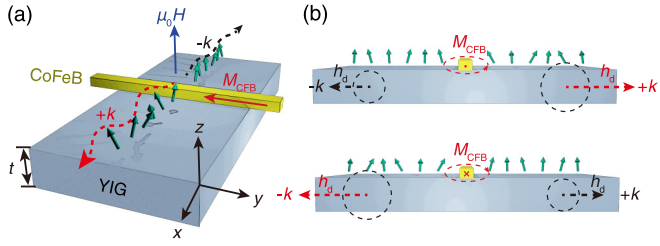

FIG. 1. (a) Illustrative diagram of the device structure. A single CoFeB nanowire is patterned on a PMA YIG film with a thickness of t. By applying an out-of-plane external magnetic field, the CoFeB nanowire excites nonreciprocal propagating short-wavelength forward volume spin waves in the PMA YIG thin film. (b) Schematic of the key mechanism of the nonreciprocal forward volume spin waves excited by the CoFeB nanowire. The key physics is the interlayer dipole-dipole interaction that occurs when the CoFeB nanowire is resonating.

efficiently excite spin waves in YIG. During the device fabrication process, we realized that if the nanowire is not wide enough (width smaller than 300 nm), the measured signal for short-wavelength spin waves in YIG is relatively weak. Consequently, we choose to use nanowires that are about 600 nm wide. Interestingly, the x components of the dynamic stray dipolar fields generated by CoFeB nanowire magnetization at resonance are inherently chiral at $\pm x \parallel k$ directions [49,51], which implies that the x components of the stray fields, generated from the two orthogonal components of the precessing magnetization in the CoFeB nanowire, Δm_x and Δm_z, are symmetric and antisymmetric, respectively, on either side of the nanowire center $x = 0$ [Fig. 1(b)]. Detailed sketches of the dipolar field lines and symmetries are provided in Appendix D. We can describe the Fourier components of the dipolar stray field generated by the precession of the nanowire as [51]

$$\begin{aligned}\tilde{h}_x(k_x, z, t) &= \int h_x(\mathbf{r}, t) e^{-ik_x x} dx \\ &= -\frac{i}{4\pi} e^{|k_x|z}(1 - e^{-|k_x|d}) \\ &\quad \times \frac{2\sin(k_x w/2)}{k_x|k_x|}(ik_x \Delta m_z - |k_x|\Delta m_x) e^{-i\omega t}, \quad (2)\end{aligned}$$

where the Δm_x and Δm_z are the dynamic magnetization components of the CoFeB nanowires and follow $\Delta m_x = i\mathcal{D}\Delta m_z$. For $\pm k$ directions, $\tilde{h}_x \propto (1 \mp \mathcal{D})k_x \Delta m_z$. Based on these expressions, if the precession of the CoFeB can be made perfectly circular ($d = w$, $\Delta m_x = i\Delta m_z$, $\mathcal{D} = 1$), x components of stray dipolar fields will only appear on one side of CoFeB nanowire. This effect is chiral with respect to the normal vector n, the wave vector k, and the magnetization direction of the CoFeB nanowire. Here, besides the chirality imposed by the dipolar coupling at small distances, the intrinsic helicity (right-handed or left-handed) of the spin waves plays a role (see Appendix D). One important experimental consequence of the dipolar chirality is that the helicity of the spin waves can be reversed by switching the magnetization in the CoFeB nanowires as shown in Fig. 1.

III. RESULTS AND DISCUSSION

To verify the nonreciprocal excitation in the experiments, we fabricated two 600-nm-wide CoFeB nanowires on the top of PMA YIG with a separation distance of about 2 μm. Before we measured the spin-wave spectra with out-of-plane fields, we first used a large in-plane field to saturate the CoFeB nanowires along the y directions to prevent the formation of any spin texture in CoFeB nanowires when we apply out-of-plane fields. The dimensions of the CoFeB nanowires were 600 nm × 100 μm × 30 nm in the xyz directions. Therefore the large in-plane shape anisotropy field of nanowires can keep the magnetization mainly in plane when we apply an out-of-plane field with strength below 200 mT. This was verified by measuring the FMR in the CoFeB nanowires as a function of perpendicular (z axis) magnetic field. During the measurements, we swept the external magnetic fields from −150 to +150 mT with a step of 1 mT along the z direction. At each field strength, a fixed reference spectra is subtracted. This subtracted spectrum was measured at high field, where no resonance is detected. This allows us to have a cleaner baseline. In the reflection spectra (see Appendix E), one can observe two clear modes: One is the FMR of the PMA YIG mode with frequency below 5 GHz; the other mode is around 9 GHz and is almost insensitive to the out-of-plane fields within ±100 mT.This second mode is clearly from the CoFeB because it has a broad linewidth. The flat behavior of the frequency as a function of the field thus indicates that out of plane is the hard axis for the CoFeB nanowires. As shown in Figs. 2(a) and 2(b), S_{12} ($+k$) and S_{21} ($-k$) present the coherent propagation of the FV spin waves, where the clear phase oscillations are induced by the phase delay during the propagation process. Around 8 GHz, one can also observe a weak flat mode under the oscillations, which is the CoFeB nanowire resonance. A salient feature is that the transmission amplitudes are nonreciprocal between opposite directions ($\pm k$) but the same for different YIG magnetization directions ($\pm\mu_0 H_{\text{ext}}$) [Fig. 2(c)]. To have a better observation, we extracted two line plots from S_{12} and S_{21} when the external magnetic field was fixed at +100 mT. The FMR frequency of the FV mode is about 4.5 GHz at +100 mT, below which the signal is coming from the instrumental background, mainly. Above the FMR frequency, one can find that both the amplitude and nonreciprocity are strongly enhanced once the CoFeB nanowires are resonating, indicating the achievement of nonreciprocal FV propagating spin waves in very thin YIG, which inherently possesses reciprocity in the FV mode configuration. In addition to the amplitude, it seems that the frequency nonreciprocity in the transmission spectra, which has been reported before in a coupled bilayer system with antiparallel coupling in the Damon-Eshbach geometry [48,54,69,70], is not distinct. As expected, the mechanism of the nonreciprocal excitations of the FV spin waves is related to the stray field nonreciprocity generated by the CoFeB nanowire (Appendix D), which reverses its sign when the magnetization of the CoFeB is reversed. To demonstrate this, we performed a comparison measurement after saturating the magnetization of CoFeB along the $-y$ direction rather than along the $+y$ direction, before carrying out transmission measurements with out-of-plane fields [Figs. 2(d) and 2(e)]. The nonreciprocal

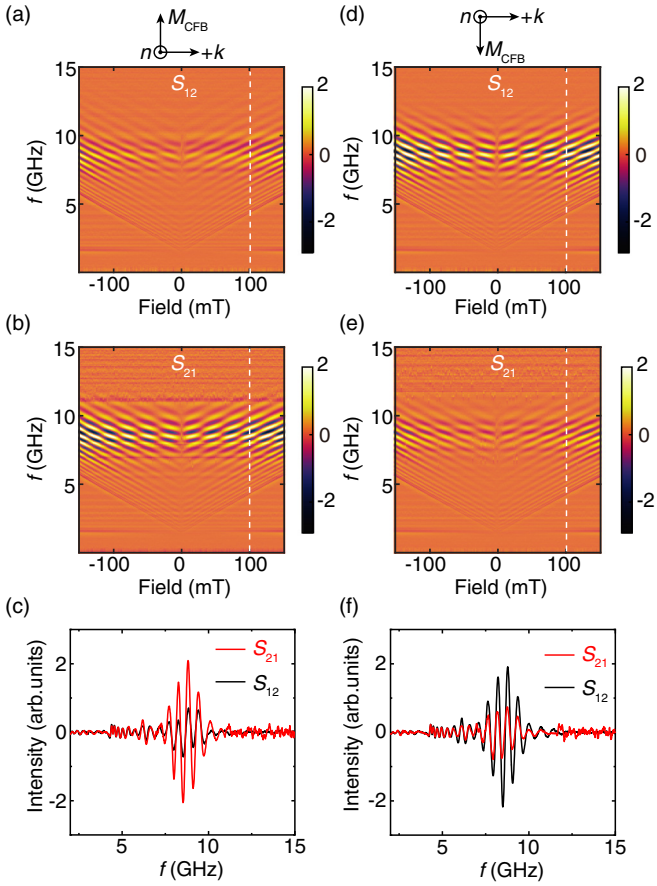

FIG. 2. (a) and (b) Spin-wave transmission spectra S_{12} and S_{21} when the CoFeB nanowire magnetizations M_{CFB} are pointing in the $+y$ direction. (c) The line plots extracted from (a) and (b) when the out-of-plane external magnetic field is $+100$ mT. (d) and (e) Spin-wave transmission spectra S_{12} and S_{21} when the CoFeB nanowire magnetizations M_{CFB} are pointing in the $-y$ direction, which is opposite from the direction in (a) and (b). (f) The line plots extracted from (d) and (e) when the out-of-plane external magnetic field is $+100$ mT.

amplitudes for opposite directions are reversed [Figs. 2(c) and 2(f)] compared with the results when the magnetization of the CoFeB is saturated along the $+y$ direction, indicating that the nonreciprocal amplitudes of the FV spin waves can be reconfigurable by switching the in-plane magnetization of the CoFeB nanomagnets.

Our data provide us the possibility to estimate the dispersion of exchange waves, using the following approach. We use the fact that the spin-wave group velocity is the derivative of the dispersion and can be estimated from the phase oscillations in the transmission spectra by using the empirical formula [71–73]

$$v_g = \frac{\partial \omega}{\partial k} \approx \frac{2\pi \Delta f}{\Delta k} = \frac{2\pi \Delta f}{2\pi / s} = s\Delta f, \tag{3}$$

where s is the propagation distance and Δf is the frequency difference between two neighboring peaks with 2π phase changing. The spin-wave group velocities [Fig. 3(a)] are extracted as a function of the frequencies for opposite propagation directions S_{21} (red open circles) and S_{12} (black

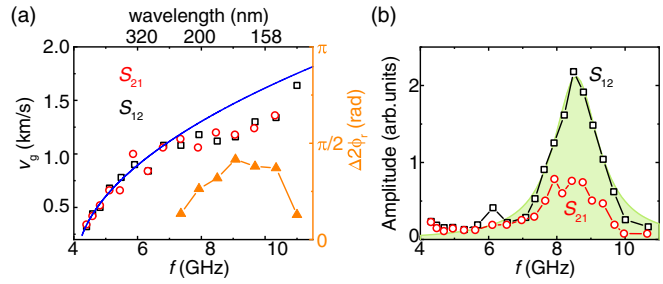

FIG. 3. (a) The spin-wave group velocity as a function of the frequencies for S_{12} (black open squares) and S_{21} (red open circles) measurements (see Fig. 1), where the blue solid curve is the fitting using Eq. (4). The orange triangles are the dissipative phase difference between two neighboring peaks ($\Delta\ 2\phi_r$) extracted from the experimental results. (b) The amplitudes as a function of the frequencies for S_{12} (black open squares) and S_{21} (red open circles), where the light green background is the fitting of the imaginary part of the complex magnetic susceptibility under the CoFeB nanowire FMR condition [see Eq. (7)].

open squares), and the velocities are increasing for higher frequencies. The relationship between them can be fitted by the dispersion equation of dipole-exchange spin waves in the FV mode configuration as [2,74,75]

$$f_{FV} = \frac{|\gamma|\mu_0}{2\pi}\left[\left(H_{ext} + M_{eff} + \frac{2A}{\mu_0 M_s}k^2\right)\right.$$
$$\left.\times\left(H_{ext} + M_{eff} + \frac{2A}{\mu_0 M_s}k^2 + M_s\left(1 - \frac{1-e^{-kt}}{kt}\right)\right)\right]^{\frac{1}{2}}, \tag{4}$$

where $|\gamma| = 2\pi \times 28$ GHz/T is the gyromagnetic ratio; t is the thickness of the YIG film, about 30 nm; $\mu_0 M_{eff} = \mu_0 H_{ani} - \mu_0 M_s$ is the effective magnetization; and $\mu_0 H_{ani}$ is the perpendicular anisotropy field. Based on the results of reflection spectra shown in Appendix E, we can obtain that the $\mu_0 M_{eff}$ of our PMA YIG film is about 52 mT. Thus, by fitting the extracted group velocities as a function of frequencies to $v_g = \partial(2\pi f_{FV})/\partial k$ using Eq. (4), we can estimate that the exchange stiffness constant A is about 3.8×10^{-12} J/m and the saturation magnetization of 30-nm-thick PMA YIG is about 180 ± 5 mT, indicating that $\mu_0 H_{ani}$ is about 232 mT.

As shown in Fig. 3, we find that the fitted curve and experimental results are matched well with each other when the frequency is below the resonance frequency of CoFeB nanowires. Once the frequency is close to the resonating regime of CoFeB nanowires, the extracted group velocities deviate from the fitting curve. These differences are due to an additional phase ϕ_r of the propagating FV spin-wave transmission in YIG provided by the CoFeB resonance [13,51]. The total phase of spin waves in YIG can be described as $\phi_{total} = 2\phi_r + \phi_k$, where $\phi_k = ks$ is the conventional propagating phase delay and $2\phi_r$ is twice the dissipative phase shift induced by the resonance of the CoFeB nanowires. This phase shift applies twice because it occurs when the propagating spin waves in YIG are excited from CoFeB and detected from YIG by the CoFeB. This additional phase shift can be

described by the magnon Green's function [13,51]

$$2\phi_r = 2\arg\left(\frac{1}{(\omega_{\mathrm{CoFeB}} - \omega) + i\Gamma_{\mathrm{CoFeB}}/2}\right), \tag{5}$$

where $\Gamma_{\mathrm{CoFeB}} = 2\omega_{\mathrm{CoFeB}}\alpha_{\mathrm{eff}}$ is the dissipative term of the CoFeB Kittel mode and α_{eff} is its effective damping, not the intrinsic one. When the frequency ω matches the resonance frequency of the CoFeB nanowire ω_{CoFeB}, only the dissipative term is left in the denominator of Eq. (5) for ϕ_r, leading to a $\pi/2$ phase shift. Once the frequency is larger than the CoFeB resonance frequency, the additional phase ϕ_r provided by the nanowire to the spin waves in YIG is π. Therefore, in the frequency range around the resonance of CoFeB in Fig. 3(a), the phase difference 2π between two neighboring peaks in the transmission spectra can also have a contribution from $2\phi_r$ ranging from 0 to 2π as the frequency is varied,

$$v_g^{\mathrm{real}} \approx \frac{2\pi\,\Delta f}{\Delta k^{\mathrm{real}}} = \frac{2\pi\,\Delta f}{(2\pi - \Delta 2\phi_r)/s}, \tag{6}$$

where $\Delta 2\phi_r = 2\phi_r(f_2) - 2\phi_r(f_1)$ is the additional phase difference between two neighboring peaks with frequencies f_1 and f_2 in the transmission spectra. From the experimental results, we extracted the dissipative phase difference ($\Delta 2\phi_r$) at different pairs of frequencies of two neighboring peaks [orange triangles in Fig. 3(a)], and the sum of these additional phase difference is equal to 2π, which is consistent with the results in Fig. 3(b). This explains the difference between the extracted group velocities and their fitted curve when the frequency is larger than 6.0 GHz in Fig. 3. The propagating signal vanishes once the frequency is higher than the CoFeB resonance frequency range because the CoFeB nanowire is not resonating and cannot provide significant stray field to excite the short-wavelength spin waves in YIG. By using the dispersion equation (4), we find that the highest frequency [around 11 GHz in Fig. 3(a)] corresponds to a wavelength of 150 nm. In addition to the group velocities, we also extract from our data the amplitudes of the opposite propagation directions as a function of frequency [Fig. 3(b)]. The strengths of the FV spin waves propagating in both directions in YIG are strongly enhanced when the CoFeB magnetization is resonant. At the peak of the amplitude of S_{21}, the nonreciprocity also achieves its maximum value. We define the nonreciprocity parameter β as A_{12}/A_{21}, which is about 2.9 at the frequency with maximum strength of S_{12} and S_{21} (8.5 GHz) in Fig. 2. The extracted nonreciprocity value obtained in this paper is comparable to the typical values of approximately 4–5 observed in nonuniform excited MSSW modes measured through spatially resolved Brillouin light-scattering spectroscopy and time-resolved spin-wave spectroscopy [76–78]. In addition, it is smaller than the nonreciprocity observed in the MSSW-like mode under an out-of-plane field in the Ta/Py system, which can reach values up to 60 [68]. However, it is an experimental demonstration of nonreciprocal exchange forward volume propagating spin waves, which should inherently be reciprocal in nature. The nonreciprocal features in the YIG/CoFeB nanowire system can be accounted for by the imaginary part of the complex magnetic susceptibility under the FMR condition, which can be described as [2]

$$\Delta m \propto \chi''(\omega) = \alpha_{\mathrm{eff}}\omega\omega_{\mathrm{M}}\left[\frac{\left(\omega_{\mathrm{res}}^2 - \omega^2\right) + [\omega_{\mathrm{H}} + (N_z - N_x)\omega_{\mathrm{M}}][2\omega_{\mathrm{H}} + (N_y + N_z - 2N_x)\omega_{\mathrm{M}}]}{\left(\omega_{\mathrm{res}}^2 - \omega^2\right)^2 + \alpha_{\mathrm{eff}}^2\omega^2[2\omega_{\mathrm{H}} + (N_y + N_z - 2N_x)\omega_{\mathrm{M}}]^2}\right], \tag{7}$$

where α_{eff} is the effective damping of the CoFeB nanowires, $\omega_{\mathrm{M}} = \gamma\mu_0 M_{\mathrm{s}}$, $\omega_{\mathrm{H}} = \gamma\mu_0 H_{\mathrm{ext}}$, ω_{res} is the resonance frequency of the CoFeB nanowire, and $N_x \simeq 0.065$, $N_y \simeq 0$, and $N_z \simeq 0.935$ are the demagnetization parameters provided by the dimensions of the CoFeB nanowires [79]. By fitting the amplitude in Fig. 3(b) (the light green background), we estimate that the effective damping of the CoFeB nanowire is about 0.03, the resonance frequency is about 8.6 GHz at 100 mT out-of-plane applied field, and $\mu_0 M_{\mathrm{s}}$ is about 2.1 T.

To better understand and verify this reconfigurable nonreciprocal feature in this system, we performed micromagnetic simulations [using Object Oriented Micromagnetic Framework (OOMMF)] [80]. In the simulation, the size of the YIG film is 10 μm × 5 μm × 30 nm in the *xyz* directions, and the CoFeB nanowire is set at the center of the YIG film with dimensions of 680 nm × 5 μm × 30 nm in the *xyz* directions. The size of each simulation unit cell is 5 × 5 × 30 nm. The saturation magnetizations of the CoFeB and YIG are 1450 and 140 kA/m, the exchange stiffness constants of CoFeB and YIG are 13 and 3.8 pJ/m, and the dampings for CoFeB and YIG are 0.03 and 0.0024, respectively. The effective perpendicular anisotropy of the YIG thin film is about 6 kJ/m^3. The parameters for CoFeB and YIG used in this paper are adopted from previous simulation literature [10,81,82], and these values are also consistent with the values extracted from the present measurements, as discussed above. Before the simulation in which we apply OOP external magnetic fields, we also applied in the simulation an in-plane field with strength +500 mT to saturate the magnetization of the CoFeB nanowire along the $+y$ direction. Then, we applied an out-of-plane external magnetic field of +100 mT to relax and saturate the YIG thin film. An excitation pulse field with uniform strength between 0 and 20 GHz is only applied on the CoFeB nanowire, $\mu_0 H_{\mathrm{ex}} = \mu_0 H_0 \sin(2\pi \times 20\ \mathrm{GHz}(t - 100.1\ \mathrm{ps}))/(2\pi \times 20\ \mathrm{GHz}(t - 100.1\ \mathrm{ps}))$ with $\mu_0 H_0$ of 2.0 mT in the linear excitation regime. With the help of fast Fourier transformation (FFT) of the time-domain simulation data, we obtained that the resonance frequency of CoFeB is 8.7 GHz. To investigate the nonreciprocal excitation feature, we fixed the excitation frequency at the resonance frequency of the CoFeB nanowire (8.7 GHz) to only excite the nanowire. Correlatively, its dipolar stray field excites propagating FV spin waves in the YIG thin film. As depicted in Fig. 4(a), we present a snapshot of the Δm_x component of the YIG layer. Notably, this snapshot reveals an amplitude nonreciprocity feature that aligns with the experimental observations. The origin of this feature is the nonreciprocal dynamic stray fields in the x direction, h_x, generated by the

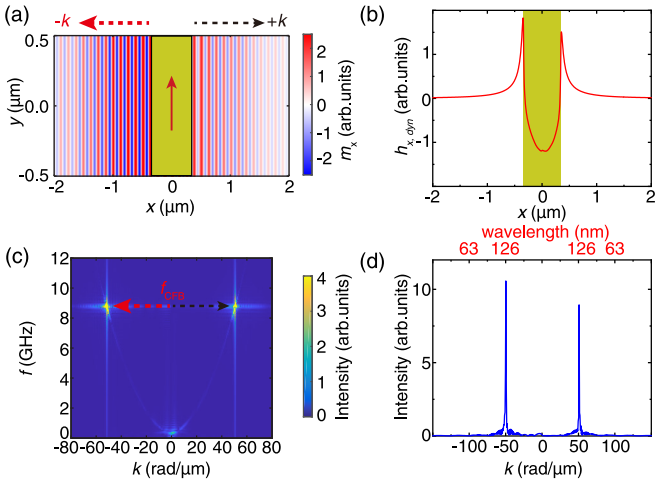

FIG. 4. (a) Spatial spin-wave snapshot of the x magnetization component when the CoFeB nanowire magnetization is along the $+y$ direction. (b) Spatial dynamic dipolar stray field h_x snapshot under the nanowire after subtracting the static stray field. (c) Micromagnetic simulation results of the dispersion relation, where the excitation frequency is fixed at the resonance frequency 8.6 GHz of the CoFeB nanowire. (d) The spectrum line plot as a function of k extracted from (c) at the fixed excitation frequency (blue curve), from which one can find that the amplitude of the $-k$ peak is stronger than that of the $+k$ peak.

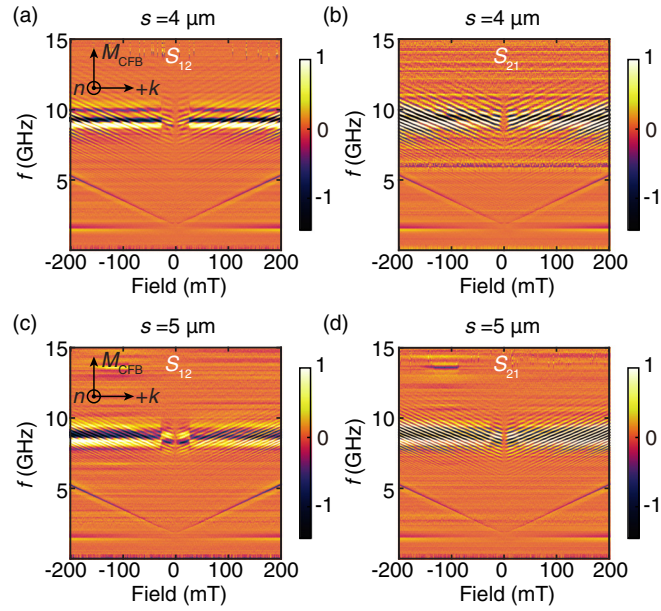

FIG. 5. [(a)–(d)] Spin-wave transmission spectra S_{12} and S_{21} measured on the device with propagation distances of 4 and 5 μm when the CoFeB nanowire is saturated along the $+y$ direction.

CoFeB nanowire resonance, which is plotted as a function of x in Fig. 4(b). In view of the wave vector space [Fig. 4(c)] calculated by the FFT of all unit cells and time steps along the x axis, the magnons ($k = 0$) in CoFeB generate magnons in YIG thin film in both $+k$ and $-k$ directions with energy conservation [Fig. 4(c)]. A line plot across the wave vector space at the CoFeB resonance frequency is extracted and presented in Fig. 4(d) with nonreciprocity strengths at $\pm k$ (blue curve). Thus, based on the simulation results, we further confirm that the nonreciprocal excitations of the propagating FV exchange spin waves in PMA YIG are induced by the intrinsically asymmetric, dynamic stray fields of the CoFeB nanowire.

Last, we fabricated a series of devices with different propagation distances up to 5 μm to verify the robustness of the nonreciprocally excited propagating FV exchange spin waves at long distances. In Figs. 5(a)–5(d), transmission spectra with opposite directions measured on the 4- and 5-μm-separated devices show the same nonreciprocal feature as we discussed above. The CoFeB nanowire Kittel mode is located around 8.5 GHz with similar linewidth of the resonance, and similar insensitivity with respect to the small out-of-plane external magnetic fields that are applied. It is worth noting that there are possibly some spin textures existing in the CoFeB nanowires when the external field is within ±20 mT, with the consequence that the phase and strength of the FV exchange spin waves in YIG thin films are affected correspondingly.

IV. CONCLUSION

In summary, we experimentally achieve the nonreciprocal excitation of propagating FV exchange spin waves in low-damping PMA YIG thin film by using in-plane magnetized CoFeB nanowires as antennas. The nonreciprocity of the excitation can be reconfigured by switching the in-plane magnetization of the CoFeB nanowire. As deduced from the spin-wave transmission spectra, the nonreciprocity reaches a maximum value of about 2.9 around the resonance frequency of the CoFeB nanowire, where the strengths of the propagating FV exchange spin waves are also strongly enhanced. By using this technique, FV exchange spin waves are found to present fast group velocities of up to 1.65 km/s, and the wavelengths are down to 150 nm in the experiments. Combined with micromagnetic simulations, we understand the experimentally observed results and verify that the key physics at play is the asymmetric dynamic stray field generated by the CoFeB nanomagnet resonance. At last, distance-dependent measurements show that the features are still available at long distances, up to 5 μm. By systematically varying the ratio between width and thickness of the nanowire, unidirectional excitations of FV exchange spin waves could be achieved in further works. Our approach offers a promising platform for the development of low-power and reconfigurable spin-wave-based devices with nonreciprocal and tuneable characteristics and proposes a method to measure nanowire magnon mode helicities (right-handed or left-handed) by their asymmetric dipolar stray fields.

ACKNOWLEDGMENTS

We wish to acknowledge support from the National Key Research and Development Program of China under Grant No. 2022YFA1402801, NSF China under Grants No. 12074026 and No. U1801661, the China Scholarship Council (CSC) under Grant No. 202206020091, and the Shenzhen Institute for Quantum Science and Engineering, Southern University of Science and Technology

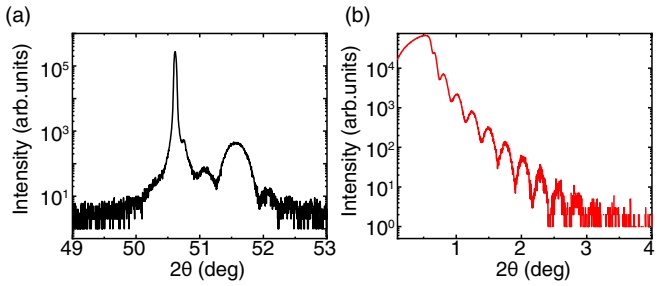

FIG. 6. The XRD (a) and XRR (b) results measured on 30-nm-thick PMA YIG thin film.

(Grant No. SIQSE202007). W.L. acknowledges support from an ETH Zurich Postdoctoral Fellowship (21-1 FEL-48).

APPENDIX A: XRD AND XRR RESULTS MEASURED ON PMA YIG THIN FILM

In Fig. 6, we report XRD and XRR measurements to characterize the crystal quality of the 30-nm-thick PMA YIG thin film. As shown in Fig. 6(a), the main peak at 50.46° is from the (444) of the sGGG substrate, and the second peak and its Laue fringes located around 51.43° are from the (444) of the YIG thin film, which indicates the good crystalline quality of the YIG thin film grown by sputtering. To precisely obtain the thickness of YIG, we also performed the XRR measurement as shown in Fig. 6(b), yielding a thickness of 32.0 ± 0.8 nm.

APPENDIX B: MAGNETIC HYSTERESIS LOOPS AND GILBERT DAMPING CHARACTERIZATION

The magnetic hysteresis loops presented in Fig. 7 were measured using a SQUID while applying external magnetic fields in the in-plane and out-of-plane directions. Based on the OOP loop, we can estimate that the saturation magnetization M_s is about 140 kA/m, namely, $\mu_0 M_s$ is 175 mT. The coercive field in the OOP direction is smaller than 5 mT. Then, to characterize the magnetic damping of the YIG thin film, we performed FMR measurements to obtain the linewidths at different resonance frequencies. In Fig. 7(b), the linewidths have a linear relationship with respect to the frequency. We

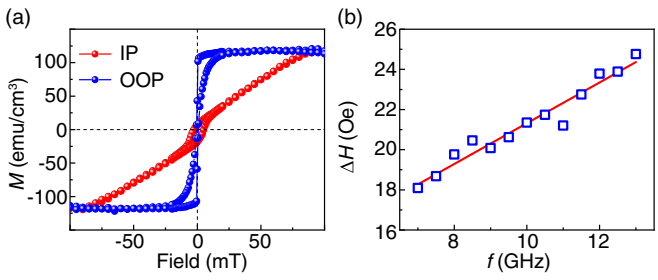

FIG. 7. (a) The IP (red) and OOP (blue) magnetic hysteresis loops of the PMA YIG measured using a SQUID. (b) FMR linewidths as a function of excitation frequencies, where the red line is the fitting for the damping and inhomogeneous linewidth extractions.

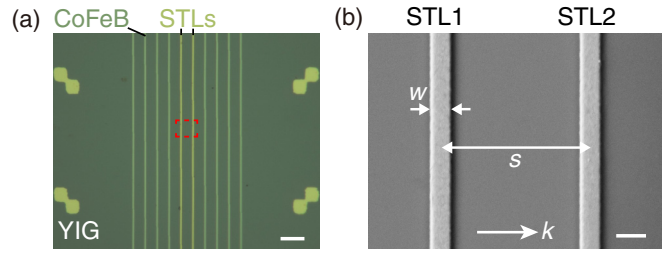

FIG. 8. (a) Optical image of the CoFeB nanowires and STL antennas on the 5-μm-separated device; the scale bar is 10 μm. (b) Zoomed-in SEM image of two STL antennas in (a); the scale bar is 1 μm.

use the following equation [2]:

$$\mu_0 \Delta H = \mu_0 \Delta H_0 + \frac{4\pi\alpha f}{\gamma}, \tag{B1}$$

where $\mu_0 \Delta H$ is the linewidth, $\mu_0 \Delta H_0$ is the inhomogeneous linewidth broadening, and α is the Gilbert damping. Through the fitting in Fig. 7(b) (red line), we estimate that the damping is about 2.36×10^{-3} in the unpatterned film and the inhomogeneous linewidth broadening is about 11 Oe.

APPENDIX C: OPTICAL AND SEM IMAGES OF THE DEVICE WITH STL ANTENNAS

The optical microscope image in Fig. 8(a) presents detailed information about the CoFeB nanowires and STL antennas in the 5-μm-separated device. At the middle of the nanowire grating, the two light yellow nanowires are the CoFeB nanowires covered by STL antennas, and the other nanowires on either side are backup CoFeB nanowires in case the middle two are broken. The scale bar in Fig. 8(a) is 10 μm. To precisely obtain the width of the antenna and nanowires, we scan the SEM images of the red dashed window range in Fig. 8(a). From Fig. 8(b), we can extract that the width of the STL antennas is about 680 nm, where the scale bar is 1 μm.

APPENDIX D: ILLUSTRATIVE DIAGRAMS OF THE NONRECIPROCAL STRAY FIELD GENERATED BY THE MAGNETIC NANOWIRE KITTEL MODE

In this Appendix, we sketch the illustrative diagrams of the asymmetric stray fields generated by the dynamic magnetization component part of the CoFeB nanowires. As present in Fig. 9(a), for example, the CoFeB magnetization is pointing out, and the precession is always right-handed in the ferromagnetic materials. We then plot the x and z dynamic magnetization components in such a way that Δm_x (orange arrows), Δm_z (black arrows), and m (the magnetic moment of the CoFeB nanowire) follow a right-handed chirality relationship. In this case, these two dynamic components will generate stray fields (the blue and green dashed curves and arrows). One can find that the x components of the stray field imposed by Δm_x are symmetric (same directions) in the $\pm k$ directions, while the ones imposed by Δm_z are the opposite. After adding these two contributions together, one can find that the x component of the stray field generated by the nanowires is stronger in one direction than in the opposite one. In addition, once the magnetization of the

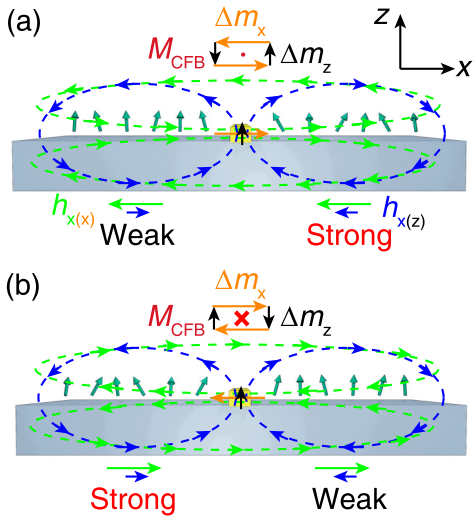

FIG. 9. (a) and (b) Illustrative diagrams of the asymmetric stray field generated by the CoFeB nanowire Kittel mode with different in-plane magnetization directions. The red point and cross are the direction of the CoFeB nanowires, the orange and black arrows indicate Δm_x and Δm_z, and the green and blue dashed lines and arrows are the stray fields generated by Δm_x ($h_{x(x)}$) and Δm_z ($h_{x(z)}$), respectively.

CoFeB nanowire is reversed, the stronger side reverses correspondingly [Fig. 9(b)]. In the specific case of a circular precession inside the magnetic nanowires, where Δm_x and Δm_z would be equal, the stray field distribution would be unidirectional.

APPENDIX E: REFLECTION SPECTRA AND YIG FV FMR FITTING

Reflection spectra, which mainly include the uniform mode of the system, are detected from the excitation antennas

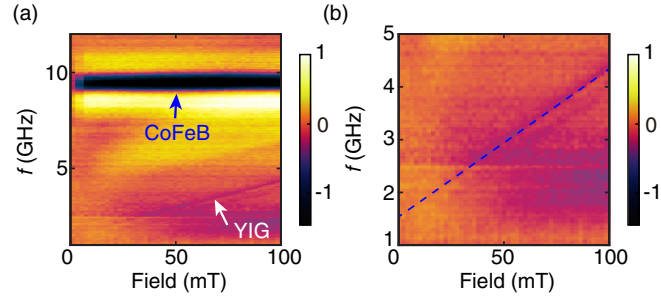

FIG. 10. (a) The reflection spectra of the CoFeB nanowires on the PMA YIG device, from which one can observe two clear modes: One is PMA YIG FV FMR, and the other is the Kittel mode of the CoFeB nanowire, the frequency of which is mostly insensitive to the external OOP fields. (b) The low-frequency zoomed-in spectra of (a), where the blue dashed line is the fitting of the PMA YIG FV FMR using Eq. (E1).

covering the CoFeB nanowire on the top of the PMA YIG film. As presented in Fig. 10(a), two modes can be clearly observed in the spectra: One is a low-frequency and low-intensity mode (the PMA YIG FV FMR), and the other, a high-frequency and high-intensity mode, is the Kittel mode of the CoFeB nanowires, the frequency of which is essentially insensitive to the external OOP magnetic fields. The PMA YIG FV FMR can be theoretically described as [2]

$$f_{\mathrm{FMR}} = \mu_0|\gamma|(H_{\mathrm{ext}} + H_{\mathrm{ani}} - M_{\mathrm{s}}). \tag{E1}$$

By using this equation, we can fit the parameter $\mu_0 M_{\mathrm{eff}} = \mu_0 H_{\mathrm{ani}} - \mu_0 M_{\mathrm{s}}$ for further fitting for the high-k spin waves. As shown in Fig. 10(b), the blue dashed line is calculated using $\mu_0 M_{\mathrm{eff}} = 52$ mT and is consistent with the experimental results.

[1] P. Pirro, V. I. Vasyuchka, A. A. Serga, and B. Hillebrands, Advances in coherent magnonics, Nat. Rev. Mater. **6**, 1114 (2021).

[2] D. D. Stancil and A. Prabhakar, *Spin Waves: Theory and Applications* (Springer, New York, 2009).

[3] A. V. Chumak, V. I. Vasyuchka, A. A. Serga, and B. Hillebrands, Magnon spintronics, Nat. Phys. **11**, 453 (2015).

[4] H. Yu, J. Xiao, and H. Schultheiss, Magnetic texture based magnonics, Phys. Rep. **905**, 1 (2021).

[5] A. Barman, G. Gubbiotti, S. Ladak, A. O. Adeyeye, M. Krawczyk, J. Gräfe, C. Adelmann, S. Cotofana, A. Naeemi, V. I. Vasyuchka, B. Hillebrands, S. A. Nikitov, H. Yu, D. Grundler, A. V. Sadovnikov, A. A. Grachev, S. E. Sheshukova, J.-Y. Duquesne, M. Marangolo, G. Csaba *et al.*, The 2021 magnonics roadmap, J. Phys.: Condens. Matter **33**, 413001 (2021).

[6] V. Kruglyak, S. Demokritov, and D. Grundler, Magnonics, J. Phys. D: Appl. Phys. **43**, 264001 (2010).

[7] G. Csaba, A. Papp, and W. Porod, Perspectives of using spin waves for computing and signal processing, Phys. Lett. A **381**, 1471 (2017).

[8] A. V. Chumak, P. Kabos, M. Wu, C. Abert, C. Adelmann, A. O. Adeyeye, J. Akerman, F. G. Aliev, A. Anane, A. Awad, C. H. Back, A. Barman, G. E. W. Bauer, M. Becherer, E. N. Beginin, V. A. S. V. Bittencourt, Y. M. Blanter, P. Bortolotti, I. Boventer, D. A. Bozhko *et al.*, Advances in magnetics roadmap on spin-wave computing, IEEE Trans. Magn. **58**, 0800172 (2022).

[9] A. Serga, A. Chumak, and B. Hillebrands, YIG magnonics, J. Phys. D: Appl. Phys. **43**, 264002 (2010).

[10] C. Liu, J. Chen, T. Liu, F. Heimbach, H. Yu, Y. Xiao, J. Hu, M. Liu, H. Chang, T. Stueckler S. Tu, Y. Zhang, Y. Zhang, P. Gao, Z. Liao, D. Yu, K. Xia, N. Lei, W. Zhao, and M. Wu, Long-distance propagation of short-wavelength spin waves, Nat. Commun. **9**, 738 (2018).

[11] J. Chen, T. Yu, C. Liu, T. Liu, M. Madami, K. Shen, J. Zhang, S. Tu, M. S. Alam, K. Xia, M. Wu, G. Gubbiotti, Y. M. Blanter,

G. E. W. Bauer, and H. Yu, Excitation of unidirectional exchange spin waves by a nanoscale magnetic grating, Phys. Rev. B **100**, 104427 (2019).

[12] P. Che, K. Baumgaertl, A. Kúkolová, C. Dubs, and D. Grundler, Efficient wavelength conversion of exchange magnons below 100 nm by magnetic coplanar waveguides, Nat. Commun. **11**, 1445 (2020).

[13] H. Wang, J. Chen, T. Yu, C. Liu, C. Guo, S. Liu, K. Shen, H. Jia, T. Liu, J. Zhang, M. A. Cabero, Q. Song, T. Sa, M. Wu, X. Han, K. Xia, D. Yu, G. Bauer, and H. Yu, Nonreciprocal coherent coupling of nanomagnets by exchange spin waves, Nano Res. **14**, 2133 (2020).

[14] Q. Wang, R. Verba, B. Heinz, M. Schneider, O. Wojewoda, K. Davídková, K. Levchenko, C. Dubs, N. Mauser, M. Urbánek, P. Pirro, and A. Chumak, Deeply nonlinear excitation of self-normalised exchange spin waves, Sci. Adv. **9**, eadg4609 (2023).

[15] G. Dieterle, J. Forster, H. Stoll, A. S. Semisalova, S. Finizio, A. Gangwar, M. Weigand, M. Noske, M. Fahnle, I. Bykova, J. Grafe, D. A. Bozhko, H. Y. Musiienko-Shmarova, V. Tiberkevich, A. N. Slavin, C. H. Back, J. Raabe, G. Schutz, and S. Wintz, Coherent excitation of heterosymmetric spin waves with ultrashort wavelengths, Phys. Rev. Lett. **122**, 117202 (2019).

[16] S. J. Hämäläinen, F. Brandl, K. J. A. Franke, D. Grundler, and S. van Dijken, Tunable short-wavelength spin-wave emission and confinement in anisotropy-modulated multiferroic heterostructures, Phys. Rev. Appl. **8**, 014020 (2017).

[17] K. Baumgaertl, J. Gräfe, P. Che, A. Mucchietto, J. Förster, N. Träger, M. Bechtel, M. Weigand, G. Schütz, and D. Grundler, Nanoimaging of ultrashort magnon emission by ferromagnetic grating couplers at GHz frequencies, Nano Lett. **20**, 7281 (2020).

[18] V. E. Demidov, M. P. Kostylev, K. Rott, J. Münchenberger, G. Reiss, and S. O. Demokritov, Excitation of short-wavelength spin waves in magnonic waveguides, Appl. Phys. Lett. **99**, 082507 (2011).

[19] A. Khitun and K. L. Wang, Nano scale computational architectures with spin wave bus, Superlattices Microstruct. **38**, 184 (2005).

[20] O. Zografos, S. Dutta, M. Manfrini, A. Vaysset, B. Sorée, A. Naeemi, P. Raghavan, R. Lauwereins, and I. P. Radu, Non-volatile spin wave majority gate at the nanoscale, AIP Adv. **7**, 056020 (2017).

[21] S. Tacchi, R. Silvani, G. Carlotti, M. Marangolo, M. Eddrief, A. Rettori, and M. G. Pini, Strongly hybridized dipole-exchange spin waves in thin Fe-N ferromagnetic films, Phys. Rev. B **100**, 104406 (2019).

[22] F. Ciubotaru, T. Devolder, M. Manfrini, C. Adelmann, and I. Radu, All electrical propagating spin wave spectroscopy with broadband wavevector capability, Appl. Phys. Lett. **109**, 012403 (2016).

[23] A. Navabi, C. Chen, A. Barra, M. Yazdani, G. Yu, M. Montazeri, M. Aldosary, J. Li, K. Wong, Q. Hu, J. Shi, G. P. Carman, A. E. Sepulveda, P. Khalili Amiri, and K. L. Wang, Efficient excitation of high-frequency exchange-dominated spin waves in periodic ferromagnetic structures, Phys. Rev. Appl. **7**, 034027 (2017).

[24] K. Baumgaertl and D. Grundler, Reversal of nanomagnets by propagating magnons in ferrimagnetic yttrium iron garnet enabling nonvolatile magnon memory, Nat. Commun. **14**, 1490 (2023).

[25] L. Sheng, M. Elyasi, J. Chen, W. He, Y. Wang, H. Wang, H. Feng, Y. Zhang, I. Medlej, S. Liu, W. Jiang, X. Han, D. Yu, J.-P. Ansermet, G. E. W. Bauer, and H. Yu, Nonlocal detection of interlayer three-magnon coupling, Phys. Rev. Lett. **130**, 046701 (2023).

[26] M. Mohseni, Q. Wang, B. Heinz, M. Kewenig, M. Schneider, F. Kohl, B. Lagel, C. Dubs, A. V. Chumak, and P. Pirro, Controlling the nonlinear relaxation of quantized propagating magnons in nanodevices, Phys. Rev. Lett. **126**, 097202 (2021).

[27] L. Korber, K. Schultheiss, T. Hula, R. Verba, J. Fassbender, A. Kákay, and H. Schultheiss, Nonlocal stimulation of three-magnon splitting in a magnetic vortex, Phys. Rev. Lett. **125**, 207203 (2020).

[28] Z. Wang, H. Y. Yuan, Y. Cao, Z. X. Li, R. A. Duine, and P. Yan, Magnonic frequency comb through nonlinear magnon-skyrmion scattering, Phys. Rev. Lett. **127**, 037202 (2021).

[29] J. Chen, J. Hu, and H. Yu, Chiral emission of exchange spin waves by magnetic skyrmions, ACS Nano **15**, 4372 (2021).

[30] V. Sluka, T. Schneider, R. A. Gallardo, A. Kákay, M. Weigand, T. Warnatz, R. Mattheis, A. Roldán-Molina, P. Landeros, V. Tiberkevich, A. Slavin, G. Schütz, A. Erbe, A. Deac, J. Lindner, J. Raabe, J. Fassbender, and S. Wintz, Emission and propagation of 1D and 2D spin waves with nanoscale wavelengths in anisotropic spin textures, Nat. Nanotechnol. **14**, 328 (2019).

[31] S. Klingler, V. Amin, S. Geprags, K. Ganzhorn, H. Maier-Flaig, M. Althammer, H. Huebl, R. Gross, R. D. McMichael, M. D. Stiles, S. T. B. Goennenwein, and M. Weiler, Spin-torque excitation of perpendicular standing spin waves in coupled YIG/Co heterostructures, Phys. Rev. Lett. **120**, 127201 (2018).

[32] K. An, V. S. Bhat, M. Mruczkiewicz, C. Dubs, and D. Grundler, Optimization of spin-wave propagation with enhanced group velocities by exchange-coupled ferrimagnet-ferromagnet bilayers, Phys. Rev. Appl. **11**, 034065 (2019).

[33] L. Liensberger, A. Kamra, H. Maier-Flaig, S. Geprags, A. Erb, S. T. B. Goennenwein, R. Gross, W. Belzig, H. Huebl, and M. Weiler, Exchange-enhanced ultrastrong magnon-magnon coupling in a compensated ferrimagnet, Phys. Rev. Lett. **123**, 117204 (2019).

[34] J. L. Chen, C. P. Liu, T. Liu, Y. Xiao, K. Xia, G. E. W. Bauer, M. Z. Wu, and H. M. Yu, Strong interlayer magnon-magnon coupling in magnetic metal-insulator hybrid nanostructures, Phys. Rev. Lett. **120**, 217202 (2018).

[35] H. J. Qin, S. J. Hämäläinen, and S. V. Dijken, Exchange-torque-induced excitation of perpendicular standing spin waves in nanometer-thick YIG films, Sci. Rep. **8**, 5755 (2018).

[36] R. Salikhov, I. Ilyakov, L. Korber, A. Kákay, R. A. Gallardo, A. Ponomaryov, J.-C. Deinert, T. V. A. G. de Oliveira, K. Lenz, J. Fassbender, S. Bonetti, O. Hellwig, J. Lindner, and S. Kovalev, Coupling of terahertz light with nanometre-wavelength magnon modes via spin-orbit torque, Nat. Phys. **19**, 529 (2023).

[37] C. W. Sandweg, Y. Kajiwara, A. V. Chumak, A. A. Serga, V. I. Vasyuchka, M. B. Jungfleisch, E. Saitoh, and B. Hillebrands, Spin pumping by parametrically excited exchange magnons, Phys. Rev. Lett. **106**, 216601 (2011).

[38] A. Houshang, R. Khymyn, H. Fulara, A. Gangwar, M. Haidar, S. R. Etesami, R. Ferreira, P. P. Freitas, M. Dvornik, R. K. Dumas, and J. Åkerman, Spin transfer torque driven higher-

order propagating spin waves in nano-contact magnetic tunnel junctions, Nat. Commun. **9**, 4374 (2018).

[39] H. Man, Z. Shi, G. Xu, Y. Xu, X. Chen, S. Sullivan, J. Zhou, K. Xia, J. Shi, and P. Dai, Direct observation of magnon-phonon coupling in yttrium iron garnet, Phys. Rev. B **96**, 100406(R) (2017).

[40] J. Chen, K. Yamamoto, J. Zhang, J. Ma, H. Wang, Y. Sun, M. Chen, J. Ma, S. Liu, P. Gao, D. Yu, J.-P. Ansermet, C. W. Nan, S. Maekawa, and H. Yu, Hybridized propagation of spin waves and surface acoustic waves in a multiferroic-ferromagnetic heterostructure, Phys. Rev. Appl. **19**, 024046 (2023).

[41] Y. Li, W. Cao, V. P. Amin, Z. Zhang, J. Gibbons, J. Sklenar, J. Pearson, P. M. Haney, M. D. Stiles, W. E. Bailey, V. Novosad, A. Hoffmann, and W. Zhang, Coherent spin pumping in a strongly coupled magnon-magnon hybrid system, Phys. Rev. Lett. **124**, 117202 (2020).

[42] Y. Li, T. Polakovic, Y. L. Wang, J. Xu, S. Lendinez, Z. Zhang, J. Ding, T. Khaire, H. Saglam, R. Divan, J. Pearson, W. K. Kwok, Z. L. Xiao, V. Novosad, A. Hoffmann, and W. Zhang, Strong coupling between magnons and microwave photons in on-chip ferromagnet-superconductor thin-film devices, Phys. Rev. Lett. **123**, 107701 (2019).

[43] J. T. Hou and L. Q. Liu, Strong coupling between microwave photons and nanomagnet magnons, Phys. Rev. Lett. **123**, 107702 (2019).

[44] X. Zhang, G. E. W. Bauer, and T. Yu, Unidirectional pumping of phonons by magnetization dynamics, Phys. Rev. Lett. **125**, 077203 (2020).

[45] T. Yu, and G. E. W. Bauer, Noncontact spin pumping by microwave evanescent fields, Phys. Rev. Lett. **124**, 236801 (2020).

[46] T. Yu, Y. X. Zhang, S. Sharma, X. Zhang, Y. M. Blanter, and G. E. W. Bauer, Magnon accumulation in chirally coupled magnets, Phys. Rev. Lett. **124**, 107202 (2020).

[47] M. Küß, M. Heigl, L. Flacke, A. Horner, M. Weiler, A. Wixforth, and M. Albrecht, Nonreciprocal magnetoacoustic waves in dipolar-coupled ferromagnetic bilayers, Phys. Rev. Appl. **15**, 034060 (2021).

[48] Y. Shiota, T. Taniguchi, M. Ishibashi, T. Moriyama, and T. Ono, Tunable magnon-magnon coupling mediated by dynamic dipolar interaction in synthetic antiferromagnets, Phys. Rev. Lett. **125**, 017203 (2020).

[49] T. Yu, Y. M. Blanter, and G. E. W. Bauer, Chiral pumping of spin waves, Phys. Rev. Lett. **123**, 247202 (2019).

[50] T. Yu, H. Wang, M. A. Sentef, H. Yu, and G. E. W. Bauer, Magnon trap by chiral spin pumping, Phys. Rev. B **102**, 054429 (2020).

[51] T. Yu, Z. Luo, and G. E. W. Bauer, Chirality as generalized spin-orbit interaction in spintronics, Phys. Rep. **1009**, 1 (2023).

[52] H. Y. Yuan, R. Lavrijsen, and R. A. Duine, Unidirectional magnetic coupling induced by chiral interaction and nonlocal damping, Phys. Rev. B **107**, 024418 (2023).

[53] J. Chen, H. Yu, and G. Gubbiotti, Unidirectional spin-wave propagation and devices, J. Phys. D: Appl. Phys. **55**, 123001 (2021).

[54] R. A. Gallardo, T. Schneider, A. K. Chaurasiya, A. Oelschlägel, S. S. P. K. Arekapudi, A. Roldán-Molina, R. Hübner, K. Lenz, A. Barman, J. Fassbender, J. Lindner, O. Hellwig, and P. Landeros, Reconfigurable spin-wave nonreciprocity induced by dipolar interaction in a coupled ferromagnetic bilayer, Phys. Rev. Appl. **12**, 034012 (2019).

[55] T. Yu and B. Zeng, Giant microwave sensitivity of a magnetic array by long-range chiral interaction driven skin effect, Phys. Rev. B **105**, L180401 (2022).

[56] K. Szulc, P. Graczyk, M. Mruczkiewicz, G. Gubbiotti, and M. Krawczyk, Spin-wave diode and circulator based on unidirectional coupling, Phys. Rev. Appl. **14**, 034063 (2020).

[57] K. Yamamoto, G. C. Thiang, P. Pirro, K.-W. Kim, K. Everschor-Sitte, and E. Saitoh, Topological characterization of classical waves: The topological origin of magnetostatic surface spin waves, Phys. Rev. Lett. **122**, 217201 (2019).

[58] M. Mohseni, R. Verba, T. Brächer, Q. Wang, D. A. Bozhko, B. Hillebrands, and P. Pirro, Backscattering immunity of dipole-exchange magnetostatic surface spin waves, Phys. Rev. Lett. **122**, 197201 (2019).

[59] M. Küß, M. Heigl, L. Flacke, A. Horner, M. Weiler, M. Albrecht, and A. Wixforth, Nonreciprocal Dzyaloshinskii-Moriya magnetoacoustic waves, Phys. Rev. Lett. **125**, 217203 (2020).

[60] X. Ma, G. Yu, S. A. Razavi, S. S. Sasaki, X. Li, K. Hao, S. H. Tolbert, K. L. Wang, and X. Li, Dzyaloshinskii-Moriya interaction across an antiferromagnet-ferromagnet interface, Phys. Rev. Lett. **119**, 027202 (2017).

[61] H. Wang, J. Chen, T. Liu, J. Zhang, K. Baumgaertl, C. Guo, Y. Li, C. Liu, P. Che, S. Tu, S. Liu, P. Gao, X. Han, D. Yu, M. Wu, D. Grundler, and H. Yu, Chiral spin-wave velocities induced by all-garnet interfacial Dzyaloshinskii-Moriya interaction in ultrathin yttrium iron garnet films, Phys. Rev. Lett. **124**, 027203 (2020).

[62] J.-H. Moon, S.-M. Seo, K.-J. Lee, K.-W. Kim, J. Ryu, H.-W. Lee, R. D. McMichael, and M. D. Stiles, Spin-wave propagation in the presence of interfacial Dzyaloshinskii-Moriya interaction, Phys. Rev. B **88**, 184404 (2013).

[63] H. T. Nembach, J. M. Shaw, M. Weiler, E. Jué, and T. J. Silva, Linear relation between Heisenberg exchange and interfacial Dzyaloshinskii-Moriya interaction in metal films, Nat. Phys. **11**, 825 (2015).

[64] J. M. Lee, C. Jang, B.-C. Min, S.-W. Lee, K.-J. Lee, and J. Chang, All-electrical measurement of interfacial Dzyaloshinskii-Moriya interaction using collective spin-wave dynamics, Nano Lett. **16**, 62 (2016).

[65] K. Vogt, H. Schulheiss, S. Jain, J. E. Pearson, A. Hoffmann, S. D. Bader, and B. Hillebrands, Spin waves turning a corner, Appl. Phys. Lett. **101**, 042410 (2012).

[66] T. Goto, K. Shimada, Y. Nakamura, H. Uchida, and M. Inoue, One-dimensional magnonic crystal with Cu stripes for forward volume spin waves, Phys. Rev. Appl. **11**, 014033 (2019).

[67] G. Talmelli, T. Devolder, N. Träger, J. Förster, S. Wintz, M. Weigand, H. Stoll, M. Heyns, G. Schütz, I. P. Radu, J. Gräfe, F. Ciubotaru, and C. Adelmann, Reconfigurable submicrometer spin-wave majority gate with electrical transducers, Sci. Adv. **6**, eabb4042 (2020).

[68] J. H. Kwon, J. Yoon, P. Deorani, J. M. Lee, J. Sinha, K.-J. Lee, M. Hayashi, and H. Yang, Giant nonreciprocal emission of spin waves in Ta/Py bilayers, Sci. Adv. **2**, e1501892 (2016).

[69] M. Ishibashi, Y. Shiota, T. Li, S. Funada, T. Moriyama, and T. Ono, Switchable giant nonreciprocal frequency shift of propagating spin waves in synthetic antiferromagnets, Sci. Adv. **6**, eaaz6931 (2020).

[70] R. A. Gallardo, P. Alvarado-Seguel, A. Kákay, J. Lindner, and P. Landeros, Spin-wave focusing induced by dipole-dipole inter-

action in synthetic antiferromagnets, Phys. Rev. B **104**, 174417 (2021).

[71] H. Yu, O. d'Allivy Kelly, V. Cros, R. Bernard, P. Bortolotti, A. Anane, F. Brandl, R. Huber, I. Stasinopoulos, and D. Grundler, Magnetic thin-film insulator with ultra-low spin wave damping for coherent nanomagnonics, Sci. Rep. **4**, 6868 (2014).

[72] H. Qin, S. J. Hamalainen, K. Arjas, J. Witteveen, and S. van Dijken, Propagating spin waves in nanometer-thick yttrium iron garnet films: Dependence on wave vector, magnetic field strength, and angle, Phys. Rev. B **98**, 224422 (2018).

[73] H. Yu, R. Huber, T. Schwarze, F. Brandl, T. Rapp, P. Berberich, G. Duerr, and D. Grundler, High propagating velocity of spin waves and temperature dependent damping in a CoFeB thin film, Appl. Phys. Lett. **100**, 262412 (2012).

[74] R. E. De Wames and T. Wolfram, Dipole-exchange spin waves in ferromagnetic films, J. Appl. Phys. **41**, 987 (1970).

[75] B. A. Kalinikos and A. N. Slavin, Theory of dipole-exchange spin wave spectrum for ferromagnetic films with mixed exchange boundary conditions, J. Phys. C: Solid State Phys. **19**, 7013 (1986).

[76] V. E. Demidov, M. P. Kostylev, K. Rott, P. Krzysteczko, G. Reiss, and S. O. Demokritov, Excitation of microwave guide modes by a stripe antenna, Appl. Phys. Lett. **95**, 112509 (2009).

[77] M. Jamali, J. H. Kwon, S.-M. Seo, K.-J. Lee, and H. Yang, Spin wave nonreciprocity for logic device applications, Sci. Rep. **3**, 3160 (2013).

[78] K. Sekiguchi, K. Yamada, S. M. Seo, K. J. Lee, D. Chiba, K. Kobayashi, and T. Ono, Nonreciprocal emission of spin-wave packet in FeNi film, Appl. Phys. Lett. **97**, 022508 (2010).

[79] A. Aharonia, Demagnetizing factors for rectangular ferromagnetic prisms, J. Appl. Phys **83**, 3432 (1998).

[80] M. Donahue and D. Porter, OOMMF Users Guide, Version 1.0, Interagency Report NISTIR 6376, National Institute of Standards and Technology, Gaithersburg, MD, September 1999, https://math.nist.gov/oommf/.

[81] S. S. Mukherjee, J. H. Kwon, M. Jamali, M. Hayashi, and H. Yang, Interference-mediated modulation of spin waves, Phys. Rev. B **85**, 224408 (2012).

[82] J. Chen, J. Hu, and H. Yu, Chiral magnonics: Reprogrammable nanoscale spin wave networks based on chiral domain walls, iScience **23**, 101153 (2020).